ELSEVIER

Journal of Nuclear Materials 276 (2000) 13–21

journal of nuclear materials

www.elsevier.nl/locate/jnucmat

# Comparative study of radiation damage accumulation in Cu and Fe

M.J. Caturla[a,*], N. Soneda[b], E. Alonso[a], B.D. Wirth[a], T. Díaz de la Rubia[a], J.M. Perlado[c]

[a] *Lawrence Livermore National Laboratory, Chemicals and Materials Science Directorate, P.O. Box 808, Livermore, CA 94551, USA*
[b] *Central Research Institute of Electric Power Industry, 2-11-1 Iwado-kita, Komae-shi, Tokyo 201, Japan*
[c] *Instituto de Fusion Nuclear, Universidad Politecnica de Madrid, Madrid, Spain*

**Abstract**

Bcc and fcc metals exhibit significant differences in behavior when exposed to neutron or heavy ion irradiation. Transmission electron microscopy (TEM) observations reveal that damage in the form of stacking fault tetrahedra (SFT) is visible in copper irradiated to very low doses, but that no damage is visible in iron irradiated to the same total dose. In order to understand and quantify this difference in behavior, we have simulated damage production and accumulation in fcc Cu and bcc Fe. We use 20 keV primary knock-on atoms (PKAs) at a homologous temperature of 0.25 of the melting point. The primary damage state was calculated using molecular dynamics (MD) with empirical, embedded-atom interatomic potentials. Damage accumulation was modeled using a kinetic Monte Carlo (kMC) algorithm to follow the evolution of all defects produced in the cascades. The diffusivities and binding energies of defects are input data for this simulation and were either extracted from experiments, the literature, or calculated using MD. MD simulations reveal that vacancy clusters are produced within the cascade core in the case of copper. In iron, most of the vacancies do not cluster during cooling of the cascade core and are available for diffusion. In addition, self-interstitial atom (SIA) clusters are produced in copper cascades but those observed in iron are smaller in number and size. The combined MD/kMC simulations reveal that the visible cluster densities obtained as a function of dose are at least one order of magnitude lower in Fe than in Cu. We compare the results with experimental measurements of cluster density and find excellent agreement between the simulations and experiments when small interstitial clusters are considered to be mobile as suggested by recent MD simulations. 

*PACS:* 02.50.N; 02.70.L; 61.43.B; 61.80; 61.72

## 1. Introduction

At low irradiation dose and temperatures below 0.3 $T_m$, where $T_m$ is the melting point, defect densities visible under transmission electron microscope (TEM) are at least one order of magnitude smaller in bcc metals than in fcc metals. This effect is observed both under self-irradiation [1] and neutron irradiation [2–4]. Moreover, significant differences in macroscopic behavior, such as e.g. differences in void swelling rates [5], are well established to exist between fcc and bcc metals. There is, therefore, a need to understand, at the most fundamental level, the origin of the difference in behavior between these two classes of materials under irradiation. While significant progress has been made in the past few years, important questions remain unanswered.

Below 0.1 dpa, most of the defects observed under TEM in irradiated Cu are in the form of stacking fault tetrahedra (SFT) [2,3]. One striking feature of these experimental measurements is the fact that the average cluster size of the SFTs remains constant during irradiation and is approximately 2 to 3 nm [2,3]. Perhaps, even more interesting, is the fact that only slight changes in the average cluster size are observed for irradiation temperatures between 25°C and 300°C [6]. These observations remain unexplained. In the case of Fe, TEM experiments following neutron irradiation up to

* Corresponding author. Tel.: + 1-925-422-8964; fax: + 1-925-422-2118.
*E-mail address:* caturla1@llnl.gov (M.J. Caturla)

0022-3115/00/$ - see front matter 
PII: S0022-3115(99)00220-2

0.1 dpa show that all clusters present, when visible, are of interstitial type [4].

Molecular dynamics (MD) simulations have revealed that for the same recoil energy both the fraction and size of self-interstitial atom (SIA) clusters present at the end of the collision cascade are larger in Cu [7–10] than in Fe [10–13]. This intrinsic clustering of SIAs in displacement cascades has also been observed experimentally in Cu irradiated at very low temperatures, below annealing stage I [14]. Another interesting experimental observation [15] is the fact that in electron irradiated Cu at 10 K, large SIA clusters form during annealing in stage II indicating that small SIA clusters may be mobile at very low temperatures as predicted by recent MD simulations [16,17]. On the other hand, no evidence for SIA cluster growth during stage II annealing has been found in bcc metals [18], but MD simulations predict that these clusters should indeed be mobile at temperatures below 10 K [13,16,17,19]. One reason for this may be the fact that bcc metals typically have high impurity content, which may hinder SIA cluster motion through trapping. Regarding vacancies, both experiments and MD simulations have revealed that while in Cu the majority are found in the form of clusters in the core of the cascades, in Fe they are not [7–13,20,21].

It may be argued that the experimental differences mentioned above must be related either to a difference in the state of clustering of the cascade-induced defects (the so-called primary damage state), or to differences in the diffusion behavior of the produced defects. Above annealing stage I, when the SIAs produced in the cascade are mobile, direct comparison between experimental observations and MD simulations is difficult. It is therefore, necessary to use a hybrid simulation model to follow the kinetics of defect diffusion, recombination, agglomeration, and migration to sinks. Rate theory models are extensively used to study defect kinetics. In recent years, these models have incorporated both intracascade clustering of defects and one-dimensional migration of interstitial clusters, in the so called 'production bias' model [22]. This model has been very successful in predicting high swelling rates at low dislocation densities observed experimentally in copper [23]. However, while powerful, these simulations suffer from the fact that the inhomogeneous spatial and temporal nature of damage accumulation is difficult to treat in the context of a mean field theory. Also, most of these models consider average values for some of the parameters, in particular, average cluster sizes, which makes the study of cluster nucleation and growth difficult. Kinetic Monte Carlo (kMC) is an intermediate step between atomistic MD simulations and mean field approximations that allows for long range migration while keeping the individual character and three dimensional distribution of the defects. Long range migration of defects from a high energy damage cascade using kMC was first simulated by Heinisch [24,25], with input obtained from MD simulations [7]. Since individual cluster sizes and types are included in the simulation, kMC is a powerful tool to study cluster nucleation and growth. However, it requires of a complete description of all possible reactions between particles, that have to be extracted from other, more fundamental methods, such as MD. Important parameters, that can be later used in simpler, more compact, rate theory models, can be calculated using kMC, such as the fraction of freely migrating defects at different temperatures, as shown by Heinisch in Cu [26–28] and Soneda and Diaz de la Rubia in Fe [13].

In this paper we used a hybrid computer simulation based on MD and kMC methods to investigate the primary damage state and the accumulation of damage in fcc Cu and bcc Fe. The linked MD/kMC simulation serves to bridge the gap between MD results on defect production during an individual collision cascade ($10^{-11}$ s) and the experimentally observed defect density as a function of dose and temperature ($\geqslant 10^3$ s). We show that both defect production in displacement cascades and subsequent defect reactions and diffusion are important in understanding and quantifying the experimentally observed differences in behavior between Cu and Fe. In Section 2 we briefly explain the kMC model and give the values of the input data used in the simulations for both Cu and Fe. The MD simulation model has been discussed extensively in the past [29]. Next we show the results of the MD simulations of defect production and the kMC simulations on damage accumulation and compare the simulation results to experimental data.

## 2. Kinetic Monte Carlo model

The use of kMC to model defect diffusion during irradiation of materials has been rather sparse in the past, but the technique dates back over thirty years and was discussed extensively by Beeler [30]. The earliest reference to this method is the work of Besco in 1967 [31]. Doran [32] and Doran and Burnett [33] carried out short-term annealing simulations of displacement cascades in fcc and bcc Fe, respectively, using a Beckman 2133 analog computer and a PDP-7 with 8K of memory. More recently, Heinisch et al. [24–28] used a Monte Carlo code named ALSOME to model the migration, agglomeration and dissociation of the defects produced by 25 keV Cu self-irradiation at different temperatures. The kMC code, BIGMAC, developed by our group, has been used to model defect escape from cascades in V [34], Fe [13], Au [35], Ni [36] and Al [37].

BIGMAC is a computationally efficient kMC program which tracks the locations of defects, impurities, and clusters as a function of time. The starting point of

these simulations is the primary damage state, that is the spatially correlated locations of vacancy and interstitials, obtained from MD simulations of displacement cascades. Each defect produced (including the clusters) has an activation energy for diffusion that can be extracted either from MD simulations or in some cases from experiments. The defects are allowed to execute random diffusion jumps (in one, two- or three-dimensions depending on the nature of the defect) with a probability proportional to their diffusivity. The temperature dependence of the defect diffusivity can be written as

$$D = D_0 \exp(-E_m/kT), \tag{1}$$

where $D$ is the defect diffusivity, $D_0$ the pre-exponential factor, $E_m$ the migration energy, $T$ the temperature of the crystal, and $k$ Boltzmann's constant. A similar form applies for dissociation rates from clusters, with $E_m$ replaced by a dissociation energy that includes the binding energy, $E_b$, of a particle to the cluster. More specifically, because the particle must migrate at least one jump distance away from the cluster to be free, the effective diffusivity for a free particle leaving a cluster is approximated to be

$$D = D_0 \exp[-(E_b + E_m)/kT]. \tag{2}$$

The BIGMAC program requires input tables of $D_0$ and $E_m$ for all mobile species, as well as the pre-factors and binding energies $E_b$ for all possible clusters. The input tables can become rather large, but the program is very flexible, as only the input tables need to be changed to study another set of conditions or even another material system.

During the simulation various kinetic processes are allowed to take place. Possible events are: (i) the dissociation of a particle from a cluster; (ii) the diffusive jump of a particle; (iii) recombination of two defects of opposite types; (iv) agglomeration of two defects of the same type; (v) annihilation of a defect at a sink; (vi) trapping or detrapping of a defect at an impurity; and (vii) the introduction of a new cascade, that is, a new PKA and all its associated vacancies and SIAs. The dissociation and migration rates are given by

$$R = (2dD/\delta^2), \tag{3}$$

where $\delta$ is the jump distance set by the lattice, $d$ is the dimensionality of the migrational mechanism, and the diffusivity, $D$, is obtained from Eqs. (1) and (2). The rate of cascade introduction is given by the dose rate of the simulated irradiation. At each time step, we randomly choose among all possible events, ensuring that events occur at the proper rate by assigning each event a probability proportional to its rate. Following each chosen event, we perform all events that occur spontaneously as a result of that event. For example, a SIA which jumps within the capture radius of an I cluster will then spontaneously join the cluster (reaction iv). In these simulations if two glissile clusters interact, that is, they are within the capture radius, they form a sessile cluster. The simulation time is incremented by the inverse of the sum of the rates for all possible events in the simulation box:

$$\Delta t = \chi \left( \sum\nolimits_i N_i R_i \right)^{-1}, \tag{4}$$

where the sum is over all possible events which can occur in the simulation box, $N_i$ is the number of particles in the box that can take part in event $i$, and $R_i$ is the rate of event $i$ from Eq. (3). $\chi$ is a random deviate that gives a Poisson distribution in the time steps. The time step increases when the number of possible events decreaes or the event rate is slower. Because a kinetic process occurs during every Monte Carlo step during a kMC run, time scales of hours can be reached with these simulations. Clearly, care must be taken to completely enumerate the relevant particles and events. Finally, another input in these simulations is the capture radius for defect interaction. In this particular simulation the jump distance, $\delta$, used for both Fe and Cu is equal to the lattice parameter. The interaction radius between defects has been defined as

$$r = r_{sph} + \delta, \tag{5}$$

where

$$r_{sph} = \sqrt[3]{\frac{3N\Omega}{4\pi}} \tag{6}$$

with $\Omega$ the atomic volume and $N$ the number of defects in the cluster. Since the stress field of single-interstitials is larger than the one of single-vacancies, a larger capture radius is considered for interstitials ($r_I$) interacting with loops (vacancy or interstitial clusters) than for single vacancies ($r_V$), $r_I = 1.15 \times r_v$, where $r_V$ is defined in Eq. (5) above. This includes a bias for the interaction of interstitials and vacancies with the microstructure.

## 3. Input data to kMC model

The values of the migration energies and pre-factors for diffusion used in this work are given in Tables 1 and 2 for Cu and Fe, respectively. For Cu, vacancy values are taken from calculations by Sabochick et al. using Dangens' copper potential [38]. Although the calculations were static and no pre-factors for defect diffusivity were obtained, Sabochick et al. deduced an attempt frequency for these defects that was used in our simulation to calculate diffusivity pre-factors, assuming a jump distance of one nearest neighbor distance. For the

Table 1
Migration energies ($E_m$) and Diffusivity pre-factors ($D_0$) for Cu defects, interstitials ($I$) and vacancies ($V$)

| Species | $E_m$ (eV) | $D_0$ (cm$^2$/s) |
|---|---|---|
| $V$ | 0.72 | 0.25 |
| $V2$ | 0.55 | 0.36 |
| $V3$ | 0.56 | 0.12 |
| $V4$ | 0.38 | 0.14 |
| $I$ | 0.13 | $2 \times 10^{-3}$ |
| $I2$ | 0.11 | $1 \times 10^{-3}$ |
| $I3$ | 0.20 | $6 \times 10^{-4}$ |
| $I4$ | 0.10 | $5 \times 10^{-4}$ |
| $I5$-Imax | 0.10 | $2 \times 10^{-3}/n$[a] |

[a] $n$: number of defects in the cluster.

Table 2
Migration energies ($E_m$) and Diffusivity pre-factors ($D_0$) for Fe defects, interstitials (I) and vacancies ($V$)

| Species | $E_m$ (eV) | $D_0$ (cm$^2$/s) |
|---|---|---|
| $V$ | 0.870 | $1.15 \times 10^{-2}$ |
| $I$ | 0.167 | $2.09 \times 10^{-3}$ |
| $I2$ | 0.083 | $7.32 \times 10^{-4}$ |
| $I3$ | 0.061 | $4.60 \times 10^{-4}$ |

case of the Cu SIA, we use the experimental value obtained from observations of defect annealing in stage IE [39] (0.1 eV), and migration energies obtained by Schober and Zeller [40] for clusters of size 2 and 3. The pre-factor used for self-interstitial migration is $2 \times 10^{-3}$ cm$^2$/s, obtained by assuming a vibrational frequency of $10^{13}$ s$^{-1}$.

For iron, Soneda and Diaz de la Rubia [13] have calculated the diffusivities of the monovacancy, mono-interstitial and di-and tri-interstitial clusters, which will be referred to as 1V, 1I, 2I and 3I respectively and the results are also shown in Table 1. Observe that the migration energies for all three interstitial cluster sizes lies between 0.06 and 0.1 eV. Small SIA clusters have been observed in atomistic simulations to form proto dislocation loops in both fcc and bcc metals with $\{1\,1\,1\}\langle 1\,1\,0\rangle$ and $\{1\,1\,0\}\langle 1\,1\,1\rangle$ slip geometry, respectively. The mechanism for thermal migration of these small SIA clusters in the absence of applied stress has been discussed extensively in recent years [9,13,19,41] and will not be dealt with in detail here. It is important to note, however, that MD studies have shown that the 2I and 3I execute basically a one-dimensional random walk along the $\langle 1\,1\,1\rangle$ direction, but with sporadic changes in direction to another $\langle 1\,1\,1\rangle$. However, the frequency of the change in migration direction of the 3I is clearly much lower than that of the 2I. In Fe, the activation energy for direction change was found to be equal to the migration energy for the 2I, but 0.4 eV higher for 3I. Effectively then, SIA clusters of size 2 diffuse in three-dimensions at all temperatures, and those of size 3 do so at elevated temperatures. Diffusion pre-factors for SIA clusters in Fe were obtained for sizes up to 20 I previously [13] and are used here. For SIA clusters larger than 3 in Cu we assume a value for the pre-factors equal to that of the single SIA divided by the number of interstitials in the cluster. This takes into account the fact that even though the activation energy for migration of clusters is constant with size, the cluster diffusivity decreases as the cluster size increases and should go to zero as the cluster (loop) grows to a network dislocation which does not move by thermal activation in the absence of an applied stress. This approach is also consistent with recent MD simulations that show that even though the cluster activation energy for migration is constant for $n > 4$, the pre-factor decreases as $n$ increases [13,16].

One key issue for KMC simulations is to determine the size at which SIA clusters may be considered mobile, i.e., which clusters form glissile dislocation loops and which do not. In Cu, continuum elasticity theory predicts that clusters form as faulted loops and unfault to form perfect glissile loops at larger sizes. Thus, using a stacking fault energy of 0.062 J/m$^2$ for Cu, continuum elasticity theory predicts the unfaulting at a loop size of $\sim$12.2 nm, corresponding to a cluster containing about 8300 defects. All clusters larger than 8000 should unfault and become prismatic (glissile) loops. However, this analysis ignores the dislocation core radius and energy and thus, is not valid for very small cluster sizes of only a few nm in size. We utilize the results of MD simulations to determine the characteristics of small interstitial clusters. Indeed, the MD simulations have shown that small interstitial clusters form with perfect Burger's vector and are highly mobile. The simulations by Osetsky et al. have shown that the high mobility of the clusters persists up to about size 60. In our simulations, we have observed the one-dimensional migration of a 38 interstitial cluster produced directly in a 20 keV cascade at room temperature. At larger sizes, the cluster mobility decreases as the perfect interstitial loops dissociate into Shockley partials separated by a stacking fault, akin to the dissociation of edge dislocations [42]. Nevertheless, in Cu, no complete MD simulations for large cluster sizes exist, and the bridge between atomistic sizes, or MD simulations, and elasticity theory has not been clearly elucidated yet.

Thus, the cut-off size at which SIA clusters are considered mobile can be taken as a parameter in these simulations. The consequences derived from selecting various values of this cut-off for clusters in Cu will be discussed later in this paper. In these simulations clusters of size between 1 and 5 are considered to diffuse in three dimensions while mobile SIA clusters larger than 5 move in a one dimensional path along a $\langle 1\,1\,0\rangle$ direction. One-dimensional migrating clusters are removed from the simulation box after traveling a distance of 1 micron. For the case of Fe, the large stacking fault energy makes

the presence of faulted loops very unlikely, and therefore all interstitial clusters in the kinetic Monte Carlo simulation are considered to be mobile (glissile) loops. However, we assume that when two glissile clusters interact they form a junction, and therefore, form an immobile cluster. If the temperature is high enough, re-arrangement of this cluster can occur becoming glissile. We consider that in this simulation, due to the low temperature, this re-arrangement cannot happen.

Sabochick et al. [43] have also studied the binding energies of small vacancy clusters in copper. We have used these binding energies for small clusters and considered the binding energy of an infinite size cluster as the formation energy of a vacancy to generate a fit to larger cluster sizes. The fitting function used is given by

$$E_b^V(n) = 1.2 - 2.1(n^{2/3} - (n-1)^{2/3}) \text{ (eV)}. \quad (7)$$

For the case of interstitial clusters, values used for sizes 3 and 4 are those calculated by Schober and Zeller [40], 1.16 eV. Due to the large value of these binding energies, no cluster dissolution is expected at the temperatures considered in this simulation (<400 K) and a constant value equal to the migration plus formation energy of SIA (2.62 eV) was used for all those clusters of interstitials larger than 4.

For Fe, several authors [13,16,19] have also calculated values for the formation energy of vacancies and interstitial clusters. Soneda and Diaz de la Rubia [13] calculated the binding energies, $E_b$, of one defect to a cluster as a function of the cluster size, $n$, considering that

$$E_b = E_f(n-1) + E_f(1) - E_f(n). \quad (8)$$

Power functions of the number $n$ of cluster members were fitted to the data. The fitted curves give a relationship between binding energy and cluster size of the type

$$E_b^I(n) = 4.33 - 5.76[n^{2/3} - (n-1)^{2/3}] \text{ (eV)}, \quad (9)$$

$$E_b^V(n) = 1.73 - 2.59[n^{2/3} - (n-1)^{2/3}] \text{ (eV)}. \quad (10)$$

The binding energies of vacancy clusters are much smaller than those of interstitial clusters, which means that vacancy clusters, as expected, are much less stable than interstitial clusters at high temperatures.

## 4. Results

In Fig. 1 we show an example of the primary damage state from 20 keV cascades in Cu and Fe as obtained

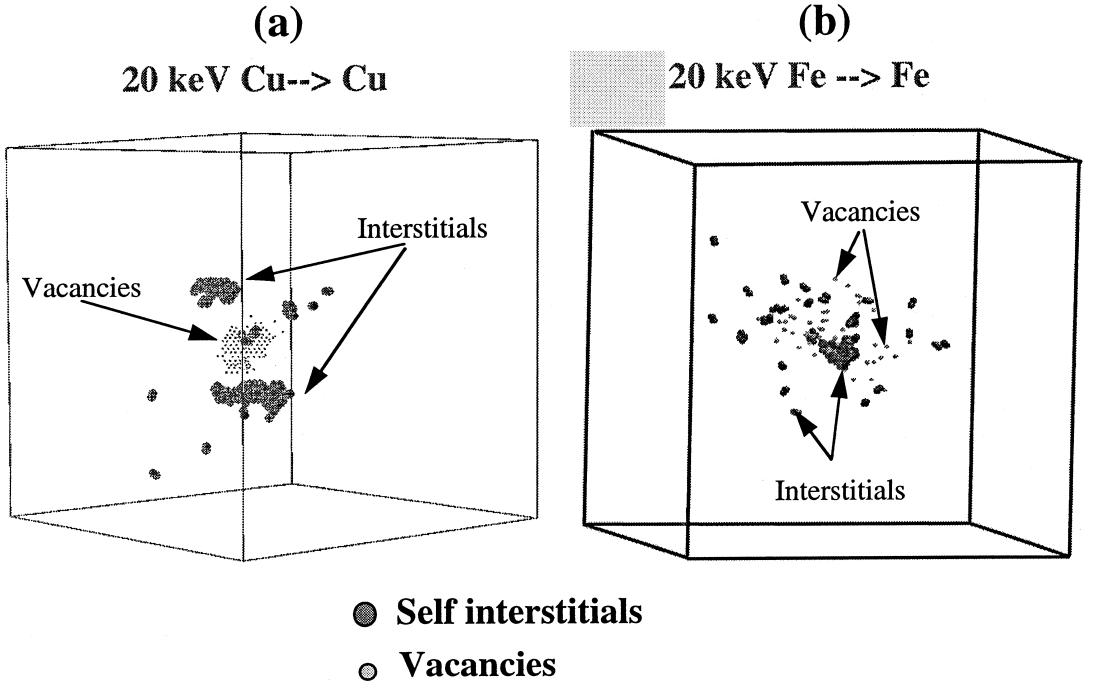


Fig. 1. Vacancies (small dots) and Interstitials (larger dots) for a 20 keV Cu cascade (a) and a 20 keV Fe cascade (b) after 10 ps of an MD simulation.

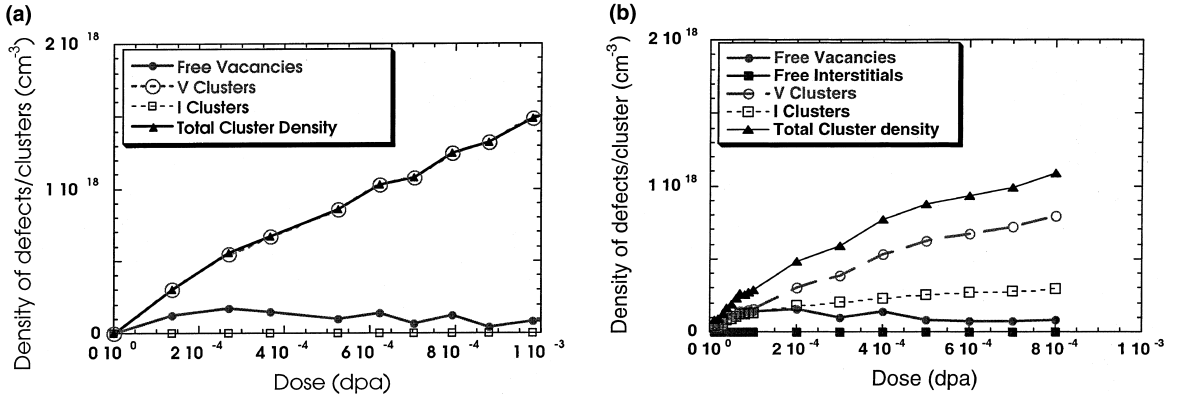


Fig. 2. Total vacancy and interstitial cluster density, and free vacancy density, for Cu (a) and Fe (b)

from molecular dynamics simulations, after approximately 10 ps. The interatomic potentials used were of the embedded atom method type [44,45]. A maximum of 20 different cascades were computed and used as a database in the KMC simulations. As expected from previous studies, the MD simulations show that at the end of the cascade cooling phase, vacancies in the core region form clusters in Cu [7] while remaining mostly isolated in Fe [12], even when considering that a cluster may be formed by vacancies as far as two nearest neighbor distances away. Not only are there more vacancy and SIA clusters in copper than in iron, the clusters are generally larger as well.

Using the primary damage state from these displacement cascades as input data, we have used our KMC simulation code BIGMAC to compute the rate of damage accumulation as a function of dose at a dose rate of $10^{-4}$ dpa/s for both metals. The temperature of the simulation was $T = 0.25T_{m'}$ that is $T^{Cu} = 340$ K and $T^{Fe} = 363$ K. In the case of Fe a total of 5 atomic parts per million (appm) of interstitial impurity atoms were included in the simulation, to take into account the high impurity content usually present in bcc metals, as opposed to the high purity of a single crystal fcc metal such as copper. The interstitial impurities in the simulation were allowed to migrate with an activation energy of 0.1 eV and to act as perfect trapping sites for SIAs and small SIA clusters.

Fig. 2 shows the SIA and vacancy cluster densities, as well as the density of free vacancies as a function of dose for Cu (Fig. 2(a)) and Fe (Fig. 2(b)). For the case of Cu all of the clusters are of vacancy type and the density increases linearly with dose. The density of free vacancies is very low and decreases with dose, as the sink strength increases, due to accumulation of vacancy clusters. In this simulation SIA clusters containing less than 60 defects are considered to be mobile, and disappear at sinks (grain boundaries, dislocations or vacancies). ~34% of the defects produced directly in the cascade recombine and this number does not change significantly with dose, which implies that most of the recombination occurs within the cascade (intra-cascade recombination), and inter-cascade recombination is very small at these low doses. This effect is due to the direct

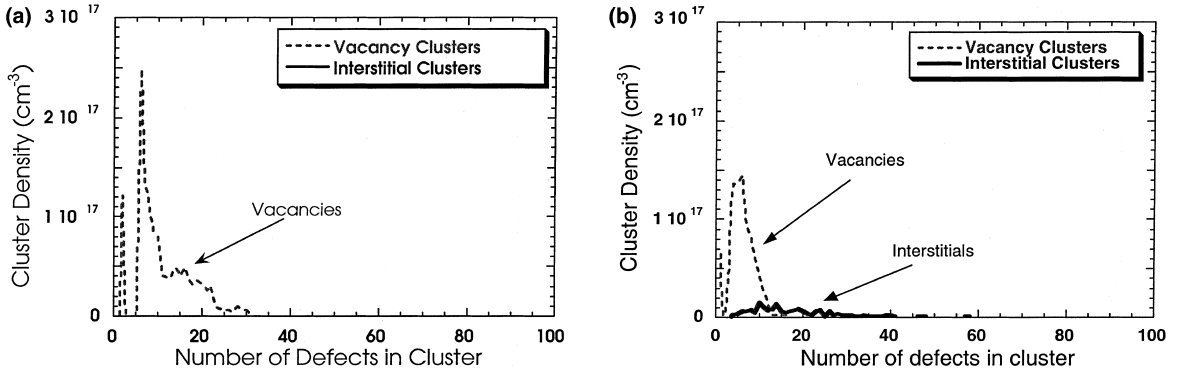


Fig. 3. Cluster size distribution for Cu (a) and Fe (b) at the same dose ($8 \times 10^{-4}$ dpa). All interstitial clusters in Cu dissappear at sinks.

formation of vacancy and interstitial clusters after the cascade collapse and the 1D migration of SIA clusters. Due to the 1D migration of SIA clusters, the recombination cross section with vacancy clusters produced in the cascade core is small. In the case of Fe the total defect density is slightly lower than in Cu and there is a significant fraction of SIA clusters.

Although the total defect densities in Cu and Fe obtained from these simulations are very similar, significant differences are observed in the cluster size distributions for these two materials. These distributions are shown in Fig. 3(a) and (b) for Cu and Fe, respectively, for a total dose of $8 \times 10^{-4}$ dpa. In the case of Cu, vacancy clusters of sizes up to 30 are obtained. The lack of smaller interstitial clusters is due to fact that they are all mobile and scape to sinks. For the case of Fe the maximum vacancy cluster is only 15, that is, half the size obtained in Cu. The SIA clusters are also small, with a maximum size of 60. These consist of both immobile clusters trapped by impurities and sessile clusters produced by the interaction of two glissile clusters.

Two important conclusions can be extracted from these simulations: (1) similar total cluster densities in Fe and Cu; (2) vacancy cluster sizes are larger in the case of Cu than in Fe for the same dose.

As mentioned earlier, the glissile/sessile interstitial cluster size used in the Cu simulations presented above was 60 interstitials. We have studied the influence of this cut-off in the final simulation results. In Fig. 4(a) we show the total cluster density for vacancies and interstitials as a function of dose for three different cut-off values between sessile and glissile interstitial clusters: 10, 40 and 60. As expected, the total number of interstitial clusters decreases and the number of vacancy clusters increases, as the cut-off for sessile clusters increases, since more clusters migrate to system sinks. The total defect density is similar for each of the three different cut-off values of sessile interstitial clusters, as shown in Fig. 4(b). It is important to note that while the total defect density in Cu is independent of the value selected for sessile SIA clusters, the balance between vacancy and interstitial clusters depends on this parameter.

## 5. Discussion

In order to compare the results from these simulations with the experimentally measured cluster densities, it is necessary to assume a minimum size that can be resolved in the experiments. A value between 1.5 and 2 nm in diameter is quoted in the literature as the minimum size resolved by TEM [2,3]. For a SFT, the edge length of the tetrahedron ($L$) containing $N_V$ vacancies is: $L^2 = N_V a_0^2 3^{1/2}/2$ where $a_0$ is the lattice parameter [46]. Then, $L = 1.5$ nm corresponds to approximately 20 defects per SFT. A three-dimensional cluster of 1 nm radius ($R$), such as a 'nano'-void, in bcc contains $N_V = 8\pi R^3/(3a_0^3)$ vacancies, thus ~350 vacancies. For a dislocation loop, the relationship between radius of the loop ($R$) and the number of defects ($N$) is $N = 4\pi R^2/(3^{1/2}a_0^2)$ for an fcc material and $N = 2^{1/2}\pi R^2/a_0^2$ for a bcc material. For a radius of 1 nm that corresponds to approximately 55 defects both in bcc and fcc. In Fig. 3(b) we have shown that in Fe all vacancy clusters are smaller than 20, and therefore not expected to be visible in the TEM. The only TEM detectable defects in the case of Fe are of interstitial type, since these grow to sizes up to 60.

Considering visible vacancy clusters as those with more than 20 vacancies and visible interstitial clusters those with more than 50 defects, we extracted the total 'visible' cluster density for Cu and Fe from the previous simulations, as we show in Fig. 5. Observe that the total defect density in Fe is more than one order of magnitude lower than in the case of Cu. All the defects in Fe are of interstitial type while all the defects in Cu are of vacancy type, in good agreement with experimental observations [2,3]. For the case of Cu, it has been reported by Zinkle et al. [3] that one half of the defect clusters formed

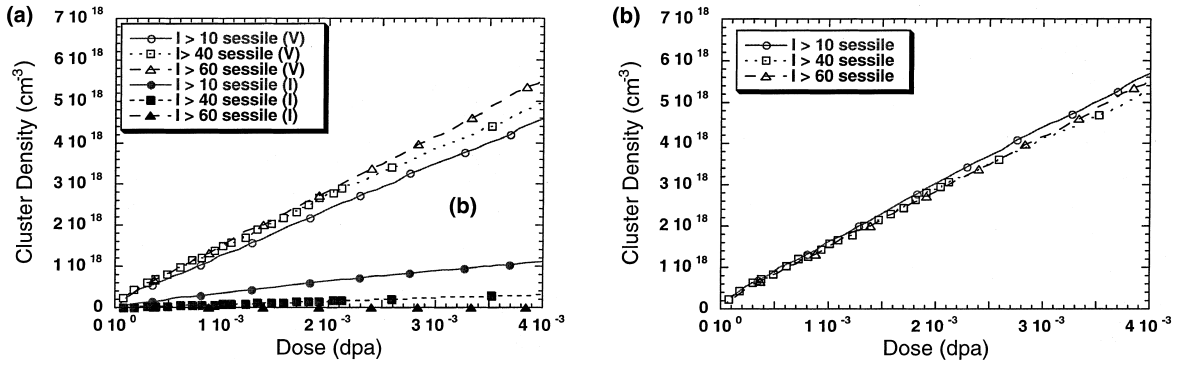


Fig. 4. Cluster density as a function of dose in Cu for different cut-off values between sessile and glissile interstitial clusters. Fig. 5(a) shows cluster density of vacancies and interstitials. The total cluster density is shown in Fig. 5(b).

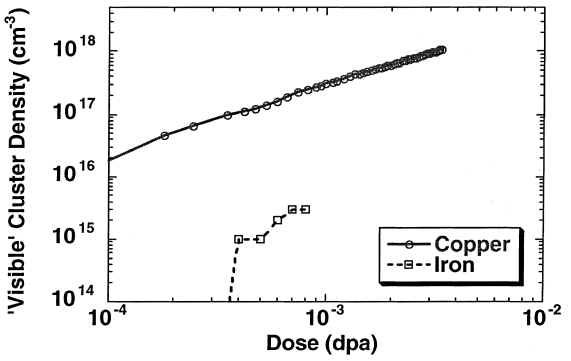


Fig. 5. 'Visible' cluster densities for Cu and Fe. Vacancy clusters are those with more than 20 defects, interstitials with more than 50.

during neutron irradiation near room temperature are resolvable as stacking fault tetrahedra. However, as the TEM technique improved the fraction of defects resolvable as SFTs increased from about 50% to 80% or more of the total cluster density [2,3], in good agreement with the fraction of 'visible' vacancy clusters obtained in the simulations presented here. As we mentioned in Section 4, the ratio between vacancy clusters and interstitial clusters depends on the cut-off selected for interstitial cluster migration. For example, a cut-off of 40 interstitials as maximum glissile cluster will result in a ratio of 70% vacancies and 30% interstitials, contradicting experimental observations. Larger cut-off for the migrating interstitial clusters are necessary in order to reproduce the experimental evidence within this simulation model.

In Fig. 6 we show the average cluster size of the vacancy clusters in Cu considering only those clusters that are larger than 20. The average cluster size remains constant over the dose range of this simulation and is independent of the selected cut-off for interstitial cluster migration. This is in good agreement with experimentally measured average clusters sizes for stacking fault tetrahedral in Cu for a large temperature range [2,3,6]. The average size in the simulation is 28 defects per cluster, which correspond to an SFT of approximately 1.8 nm. The value measured in the experiments is between 2 and 3 nm [2,3,6] . This simulation shows that these defects are actually produced in the cascade core and are not evolving in time, due to the low concentration of free vacancies at this low temperature.

In Fig. 7, we show the 'visible' cluster density for Cu as a function of dose together with the experimental results for irradiation with neutrons and protons [2]. Three different 'visible' cluster sizes were considered in this analysis: vacancy clusters with more than 10, 20 and 25 vacancies, corresponding to 1, 1.5 and 1.7 nm SFT respectively. Microscopy resolution is believed to be $\sim$1 nm. The best agreement between simulations and experiments is when clusters larger than 1.5 nm are considered as 'visible'. When smaller clusters are included, the total concentration in the simulation is above that of experiments. A quantitative comparison between experiments and simulations requires of a detail study of the microscopy resolution, in particular of the relationship between the image size, or size measured in the microscope, and the real size, and the contrast of different cluster sizes and location of the clusters in the sample. In general, the simulations results are in agreement with the experimental values, up to a dose of $\sim 10^{-2}$ dpa, when defect clusters larger than 20 are considered visible in the TEM. Overlap effects are not included in this simulation. Work is on the way in order to include these effects and extend the validity of these simulations to larger doses. We should point out the difference in dose rates between experiments and the simulations presented here. However, since the temper-

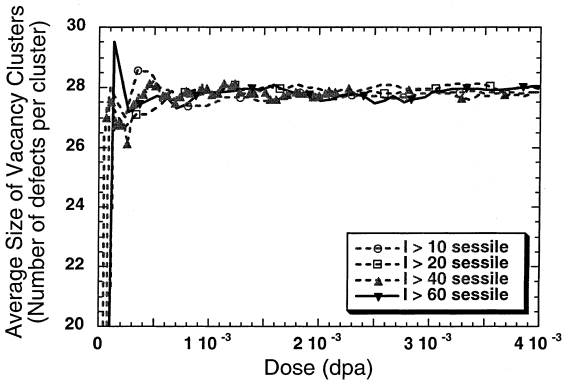


Fig. 6. Average vacancy cluster size as a function of dose for those clusters larger than 20 defects per cluster.

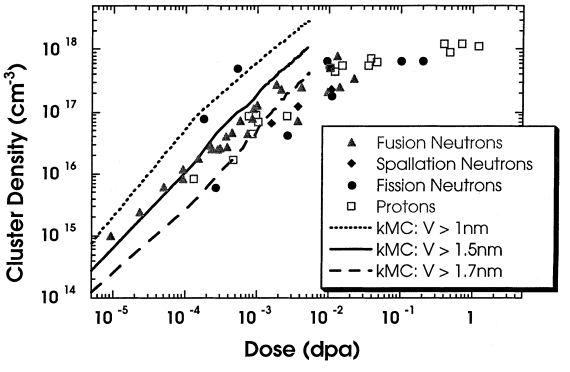


Fig. 7. 'Visible' cluster density for Cu. Comparison to experimental results under different irradiation conditions. Three cluster sizes are considered as 'visible' in the simulations: vacancy clusters larger than 1, 1.5 and 1.7 nm.

ature for irradiation is only 340 K, that is, below stage $V$, and vacancies are forming clusters, no significant difference should exist for different dose rates. This is, in fact, observed experimentally, where irradiation with neutrons or protons give very close values for total defect production, as can be seen in Fig. 7.

In conclusion, we have simulated the damage accumulated in Cu and Fe under similar conditions. We have obtained that total defect densities in Cu and Fe are very similar for the same dose. However, cluster size distributions at the same dose are very different with much larger cluster sizes in Cu than in Fe. We attribute this difference to the formation of large vacancy clusters in the cascade core in Cu, and the much larger number of free vacancies in the case of Fe. If we assume a minimum resolvable TEM cluster size of 20 vacancies in a SFT and 50 interstitials in a loop, the cluster densities in Cu are in good agreement with experiments and more than one order of magnitude higher than in Fe.

## Acknowledgements

This work was performed under the auspices of the US Department of Energy by Lawrence Livermore National Laboratory under contract W-7405-Eng-48. We have benefited from discussion with Drs S. Zinkle and Max Victoria. We thank Dr Yong Dai for providing the experimental data in Cu.

## References

[1] M.L. Jenkins, M.A. Kirk, W.J. Phythian, J. Nucl. Mater. 205 (1993) 16.
[2] Y. Dai, M. Victoria, Mater. Res. Soc. Symp. Proc. 439 (1997) 319.
[3] B.N. Singh, S.J. Zinkle, J. Nucl. Mater. 206 (1993) 212.
[4] B.L. Eyre, A.F. Bartlett, Philos. Mag. 12 (1965) 261.
[5] B.N. Singh, J.H. Evans, J. Nucl. Mater. 226 (1995) 277.
[6] S.J. Zinkle, G.L. Kulcinski, R.W. Knoll, Nucl. Mater. 138 (1986) 46.
[7] T. Diaz de la Rubia, M.W. Guinan, Phys. Rev. Lett. 66 (1991) 2766.
[8] A.J.E. Foreman, C.A. English, W.J. Phythian, Philos. Mag. A 66 (1992) 655.
[9] D.J. Bacon, A.F. Calder, F. Gao, V.G. Kapinos, S.J. Wooding, Nucl. Instrum. and Meth. B 102 (1995) 37.
[10] W.J. Phythian, R.E. Stoller, A.J.E. Foreman, A.F. Calder, D.J. Bacon, J. Nucl. Mater. 223 (1995) 245.
[11] A.F. Calder, D.J. Bacon, J. Nucl. Mater. 207 (1993) 22.
[12] R. Stoller, G.R. Odette, B.D. Wirth, J. Nucl. Mater. 251 (1997) 49.
[13] N. Soneda, T. Diaz de la Rubia, Philos. Mag. A 78 (1998) 995.
[14] B.v. Guerard, D. Grasse, J. Peisl, Phys. Rev. Lett. 44 (1980) 262.
[15] P. Ehrhart, R.S. Averback, Philos. Mag. A 60 (1989) 283.
[16] Y.N. Osetsky, D.J. Bacon, A. Serra, Philos. Mag. Lett. 79 (1999) 273.
[17] Y.N. Osetsky, M. Victoria, A. Serra, S.I. Golubov, J. Nucl. Mater. 251 (1997) 34.
[18] F.W. Young Jr., J. Nucl. Mater. 69&70 (1978) 310.
[19] B.D. Wirth, G.R. Odette, D. Maroudas, G.E. Lucas, J. Nucl. Mater. 244 (1997) 185.
[20] C.A. English, M.L. Jenkins, Mater. Sci. Forum 15–18 (1987) 1003.
[21] M.L. Jenkins, J. Nucl. Mater. 216 (1994) 124.
[22] C.H. Woo, B.N. Singh, Philos. Mag. A 65 (1992) 889.
[23] C.H. Woo, B.N. Singh, A.A. Semenov, J. Nucl. Mater. 239 (1996) 7.
[24] H.L. Heinisch, Radiat. Eff. Def. Solids 113 (1990) 53.
[25] H.L. Heinisch, B.N. Singh, T. Diaz de la Rubia, J. Nucl. Mater. 212–215 (1994) 127.
[26] H.L. Heinisch, Nucl. Instrum. and Meth. B 102 (1995) 47.
[27] H.L. Heinisch, B.N. Singh, J. Nucl. Mater. 232 (1996) 206.
[28] H.L. Heinisch, B.N. Singh, J. Nucl. Mater. 251 (1997) 77.
[29] M.P. Allen, D.J. Tildesley, On Computer Simulation of Liquids, Oxford University, Oxford, 1987.
[30] J.R. Beeler Jr., Radiation Effects Computer Experiments, North-Holland, Amsterdam, 1983.
[31] D.G. Besco, Computer Simulation of Point Defect Annealing in Metals, USA-AEC Report GEMP-644, October 1967.
[32] D.G. Doran, Radiat. Eff. 2 (1970) 249.
[33] D.G. Doran, R.A. Burnett, in: P.C. Gehlen, J.K.R. Beeler, Jr., R.I. Jafee, (Eds.), Interatomic Potentials and Simulations of Lattice Defects, Plenum, New York, NY, 1972, p. 403.
[34] E. Alonso, M.-J. Caturla, T. Diaz de la Rubia, M. Perlado, these Proceedings, p. 221.
[35] T. Diaz de la Rubia, N. Soneda, M.J. Caturla, E. Alonso, J. Nucl. Mater. 251 (1997) 13.
[36] A. Almazouzi, M.J. Caturla, M. Alurralde, T. Diaz de la Rubia, M. Victoria, Nucl. Instrum. and Meth. B (in press).
[37] A. Almazouzi, M.J. Caturla, T. Diaz de la Rubia, M. Victoria, Mater. Res. Soc. Symp. Proc., Boston 1998 (in press).
[38] M.J. Sabochick, S. Yip, N.Q. Lam, J. Phys. F 18 (1988) 349.
[39] J.W. Corbett, R.B. Smith, R.M. Walker, Phys. Rev. 114 (1959) 1452.
[40] H.R. Schober, R. Zeller, J. Nucl. Mater. 69&70 (1978) 176.
[41] B.D. Wirth, G.R. Odette, D. Maroudas, G.E. Lucas, these Proceedings, p. 33.
[42] D.J.H. Cockayne, M.L. Jenkins, I.L.F. Ray, Philos. Mag. 24 (1971) 1383.
[43] M.J. Sabochick, S. Yip, N.Q. Lam, J. Phys. F 18 (1988) 1689.
[44] S.M. Foiles, M.I. Baskes, M.S. Daw, Phys. Rev. B 33 (1986) 7983.
[45] R.A. Johnson, D.J. Oh, J. Mater. Res. 4 (1989) 1195.
[46] S.J. Zinkle, L.E. Seitzman, W.G. Wolfer, Philos. Mag. A 55 (1987) 111.